Thermoplastic starch modified with microfibrillated cellulose and natural rubber latex: A broadband dielectric spectroscopy study

Drakopoulos S. X., Karger-Kocsis J., Kmetty Á., Lendvai L., Psarras G. C.

Thermoplastic starch modified with microfibrillated cellulose and natural rubber latex: A broadband dielectric spectroscopy study

S. X. Drakopoulos[a], J. Karger-Kocsis[b,c], Á. Kmetty[b,c], L. Lendvai[b], G. C. Psarras[a*]

[a]Department of Materials Science, University of Patras,
Patras 26504, Hellas (Greece),

[b]Department of Polymer Engineering, Faculty of Mechanical Engineering,
Budapest University of Technology and Economics,
Műegyetem rkp. 3., H-1111 Budapest, Hungary,

[c]MTA–BME Research Group for Composite Science and Technology,
Műegyetem rkp. 3., H-1111 Budapest, Hungary

*to whom correspondence should be addressed
Tel.: +30 2610 969347; Fax: +30 2610 969372
E-mail: G.C.Psarras@upatras.gr

Submitted to Carbohydrate Polymers, August, 2016

Revised, October 2016

Abstract

Thermoplastic starch (TPS) biocomposites modified with cellulose microfibers and/or natural rubber were prepared via extrusion compounding. Glycerol and water served as plasticizers for starch. The dielectric properties of the TPS composites were examined via broadband dielectric spectroscopy in the temperature and frequency ranges of 30^{o}C to 65^{o}C and 0.1 Hz to 10 MHz, respectively. Each specimen was tested twice in order to study the effect of absorbed water. The hydrophobic/hydrophilic character of the modifiers governed the dielectric performance of the corresponding TPS biocomposites. Conducted analysis revealed two relaxation processes attributed to matrix-water-reinforcement interfacial polarization and glass to rubber transition of the TPS. Evaporation of water significantly affected the first process and only slightly the second one. Energy density, prior and after water evaporation, was also determined at constant field. By employing dielectric reinforcing function the contributions of water-assisted and constituents' originated interfacial phenomena could be separated.

Key words: thermoplastic starch, microfibrillar cellulose, natural rubber latex, broadband dielectric spectroscopy, water effect

1. Introduction

In the past few decades, considerable scientific interest was focused to biodegradable, ecologically friendly polymers produced from renewable resources. The development of agro-based biopolymers aims at replacing less environmentally benign synthetic polymers in a variety of applications, mostly in packaging industry (Bugnicourt, Cinelli, Lazzeri, & Alvarez, 2014; Chung et al., 2010; Lendvai, Karger-Kocsis, Kmetty, & Drakopoulos, 2016; Nafchi, Moradpour, Saeidi, & Alias, 2013; Tábi, & Kovács, 2007).

One of the most studied biobased polymer is starch, which can be found in potato, corn, rice, pea and other plants. Starch is abundant in nature, inexpensive and most importantly, biodegradable (Chung et al., 2010; Kamel, 2007; Nasseri, & Mohammadi, 2014). Starch is a polysaccharide consisting of two distinct substances of d-glucose units; amylose which is a linear macromolecule in helical three-dimensional form and amylopectin which is a branched biopolymer. Starch exhibits no thermoplastic behavior, although it can be altered to thermoplastic after suitable processing, using mechanical shear and heating in presence of suitable plasticizers (Majdzadeh-Ardakani, Navarchian, & Sadeghi, 2010; Xie, Pollet, Halley, & Avérous, 2013). The most prominent application of thermoplastic starch, at the moment, is its potential to replace synthetic polymers in packaging industry as it is completely biodegradable in water and soil (Chen & Evans, 2005; Majdzadeh-Ardakani, et al.,

2010). In addition, applications in biomedical engineering and biomedicine can also be found as TPS (sometimes with the addition of another polymer to form a polymer blend) has been suggested to be suitable as scaffold materials in bone tissue engineering and as a carrier for controlled drug release (Mano, Koniarova, & Reis, 2003).

Various plasticizers can be used into thermoplastic starch (TPS) like, sorbitol, glycerol and water. The amount of plasticizer employed in the mixture is critical for the mechanical and thermal properties, such as Young's modulus and glass to rubber transition respectively (Dean, Yu, & Wu, 2007; Karger-Kocsis, Kmetty, Lendvai, Drakopoulos, & Bárány, 2015; Kmetty, Karger-Kocsis, & Czigány, 2015; Liu, Xie, Yu, Chen, & Li, 2009; Schlemmer, Angélica, & Sales, 2010). Water can act also as a plasticizer when is added in starch granules. In fact, starch granules swell when water is added due to H-bonding between water and hydroxyl side groups of the main polymeric chain. Under the influence of mechanical shear and heat, starch becomes gelatinized starch (Lendvai et al., 2016). However, plasticized starch-based materials face humidity and temperature problems, meaning that fundamental properties like mechanical and thermal performance are highly affected. Hence, suitable reinforcing materials and modifiers need to be employed in order to enhance further these properties (Xie, et al., 2013).

One of the most efficient methods for melt compounding of thermoplastic polymers is the extrusion technique. Single- or twin-screw extruders are usually used for manufacturing polymer blends or/and reinforced polymers (Nafchi et al., 2013; Ruellan et al., 2015; Xie et al., 2013), including TPS-based ones.

Broadband Dielectric Spectroscopy (BDS) is a powerful tool for studying molecular mobility, conductivity and interfacial effects in polymers and composite

materials (Kremer & Schönhals, 2009). Dielectric measurements have been used for the characterization of relaxation processes in biobased composite materials (Arous, Ben Amor, Boufi, & Kallel, 2007; Ladhar et al., 2014).

Natural rubber (NR) is used as an engineering material for many years, both as a matrix and as modifier (Ortiz-Serna, Carsí, Redondo-Foj, & Sanchis, 2014; Siengchin, Karger-Kocsis, & Thomann, 2008). NR is a hydrophobic, non-polar, insulating material which is mainly derived from the latex of *Hevea brasiliensis* or Hevea Rubber tree (Gatos, Martínez Alcázar, Psarras, Thomann, & Karger-Kocsis, 2007; Psarras et al., 2007; Psarras, Gatos, & Karger-Kocsis, 2007; Rolere, Bottier, Vaysse, Sainte-Beuve, & Bonfils, 2016; Rose, & Steinbüchel, 2005; Siengchin, Karger-Kocsis, Psarras, & Thomann, 2008; Tanrattanakul, & Bunkaew, 2014).

Cellulose consisting of D-glucose units is a hydrophilic linear biomacromolecule with promising biodegradable and reinforcing properties (Ladhar et al., 2014; Ortiz-Serna et al., 2014). To achieve the latter, however, its microfibrillar (micronscale) or whisker (nanoscale) versions are preferred. Cellulose is also a promising reinforcement in biomedical engineering applications due to its biocompatibility (Iqbal, Kyazze, Locke, Tron, & Keshavarz, 2015). In medicine, natural rubber latex has been investigated for over 100 years on enhancing it upon biodegradation from fungi and bacteria, in order to product gloves and other medical equipment (Rose & Steinbüchel, 2005). Additionally, biomedical engineering applications employ natural rubber latex membranes as protein delivery systems in guided bone regeneration. These membranes follow a modified manufacturing process producing a much better biocompatible polymer (Herculano, et al., 2009).

In the present study, TPS biocomposites modified with microfibrillated cellulose and/or NR microparticles were prepared. The dielectric properties of the produced

biocomposites were investigated by means of BDS in the frequency range of 10^{-1} to 10^{6} Hz and temperatures varying from 30 to 65°C. Each specimen was tested twice in the same frequency-temperature profile, in order to clarify the effect of the absorbed water, and to study the influence of the hydrophilic/hydrophobic character of the employed modifiers. The latter is related to interfacial phenomena between the constituents of the composites and is connected with their ability to store energy.

2. Experimental

2.1. Materials

Commercially available native corn starch (CS) Hungramid F Meritena 100 (obtained from Brennrag Ltd., Budapest, Hungary) was used as matrix material. As plasticizers, were used glycerol (purity of 99.5% purchased from Csepp Bt., Budapest, Hungary) and distilled water. Two types of modifiers were introduced, the microfibrillated cellulose (referred to as B600): Arbocel® B 600 with average length of 60 μm, diameter of 20 μm (JRS GmbH, Rosenberg, Germany) and NR latex (denoted as Latex further on) particles: (dry content of the NR latex 60%, supplied by Varicham Ltd., Hungary). Stearic acid (purchased from ICC-Chemol Ltd., Budapest, Hungary) was used as lubricant for thermoplastic starch.

The corn starch, microfibrillated cellulose and stearic acid powders were conditioned in a Memmert HCP153 (Frankfurt, Germany) humidification chamber at 30°C and relative humidity of 50% for at least 168 hours prior to processing in order to have the same moisture content during the specimens preparation.

2.2. Methods

A premix was prepared which included a manual mixing of starch, plasticizers, lubricant and either microfibrillated cellulose or latex or both. The ratio of starch/glycerol was fixed to exactly 4:1 wt/wt in every mixture. The composition of all mixtures is indicated in Table 1. Additionally, in every mixture, 20 g water was added for every 100 g of premix (not included in Table 1). Also, 1wt % stearic acid was added as lubricant in order to avoid high pressure during the extrusion (Tábi, & Kovács, 2007).

Table 1: Composition of all employed mixtures after extrusion and samples mass difference prior and after the first thermal cycle.

Sample	Starch (wt %)	Glycerol (wt %)	MFC (wt %)	Latex (wt %)	Δm (g)
TPS	80	20	-	-	0.008
TPS+10% B600	72	18	10	-	0.006
TPS+20% B600	64	16	20	-	0.007
TPS+10% Latex	72	18	-	10	0.010
TPS+20% Latex	64	16	-	20	0.006
TPS+10% B600+10% Latex	64	16	10	10	0.007
TPS+20% B600+10% Latex	56	14	20	10	0.008

Furthermore, the premix in every mixture was melt-compounded using a twin-screw extruder (LTE 26-44, Labtech Engineering, Samut Prakarn, Thailand) with an L/D ratio of 44 and screw diameter of 26 mm. The screw velocity was 75 rpm and contained 11 heating zones (including the die) where the temperature was 85, 90, 95, 100, 100, 100, 110, 110, 120 and 120^{o}C, while the temperature of the die was also

120°C. Premix was manually transported to the extruder. The extruder had also an atmospheric vent to remove the vaporized water (at heating zone 7). After the extrusion, the pellets were conditioned again for a week and then were compression molded to sheets of 1.7 mm average thickness with a hot press machine (Teach-Line Platen Press 200E, Dr. Collin GmbH, Munich, Germany) at temperature 130°C for 2 minutes and pressure 100 bars. Specimens for testing were cut of the compression molded sheets (Ledvai et al., 2016). After their preparation, specimens were stored in small plastic bags at room temperature for short time before testing, in order to avoid the effect of any biodegradation.

2.3. Broadband dielectric spectroscopy

The electrical response of the prepared systems was investigated by means of BDS using an Alpha-N Frequency Response Analyzer, provided by Novocontrol Technologies (Hundsagen, Germany). The voltage amplitude of the applied field was kept constant at 1 V, while frequency varied from 10^{-1} to 10^{6} Hz. Isothermal scans were conducted in the temperature range from 30 to 65°C, in steps of 5°C. The employed temperature range was selected, after relative tests, in order to determine conditions where no irreversible alteration, of the examined composites, will occur. Temperature was controlled via the Novotherm system and the dielectric test cell used was the BDS-1200, parallel-plate capacitor, with two gold-plated electrodes system, all supplied by Novocontrol. Dielectric cell was kept in dry conditions prior each test in order to avoid the influence of possible humidity.

Each specimen was subjected to two identical and successive thermal cycles. The variation of specimens mass prior and after the first thermal cycle is shown in Table 1.

3. Results and Discussion

3.1. Dielectric response-effect of water molecules

The dielectric response of all mixtures is shown in Figs 1 and 2. Dielectric data are presented in terms of dielectric permittivity and electric modulus formalisms. Complex dielectric permittivity and electric modulus are defined according to Equations (1) and (2):

$$\varepsilon^* = \varepsilon' - i\varepsilon'' \quad (1)$$

$$M^* = \frac{1}{\varepsilon^*} = \frac{1}{\varepsilon' - i\varepsilon''} = \frac{\varepsilon'}{\varepsilon'^2 + \varepsilon''^2} + i\frac{\varepsilon''}{\varepsilon'^2 + \varepsilon''^2} = M' + iM'' \quad (2)$$

where, ε', ε'' and M', M'' are the real and the imaginary parts of dielectric permittivity and electric modulus respectively. Arguments for the advantages of analyzing dielectric data in terms of different formalisms have been discussed elsewhere (Tsangaris, Psarras, & Kouloumbi, 1998).

Fig. 1 depicts the variation of the real part of dielectric permittivity as a function of temperature before and after water evaporation (1st -Figs 1a,c- and 2nd -Figs 1b,d- thermal cycle respectively) at 10^3 and 10^6 Hz (Figs 1a,b and 1c,d).

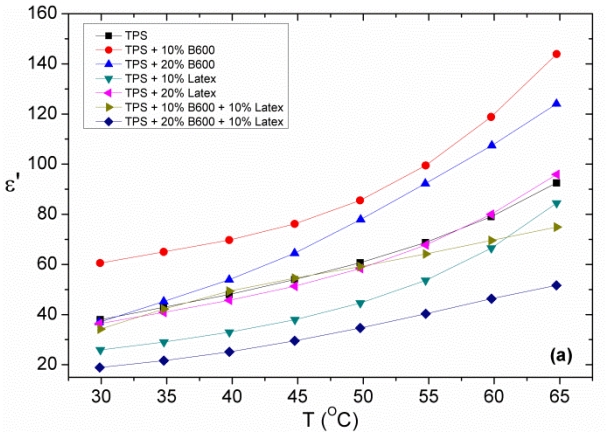

217

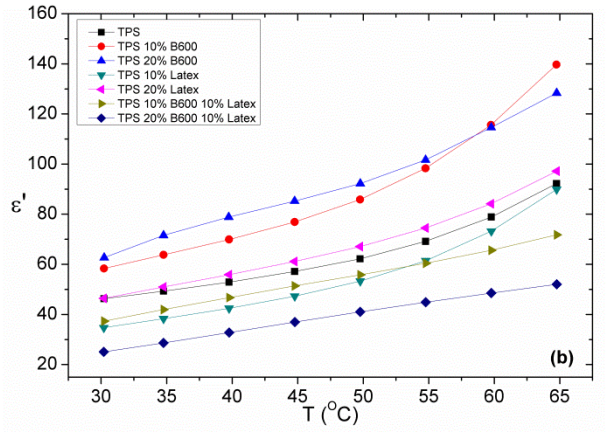

218

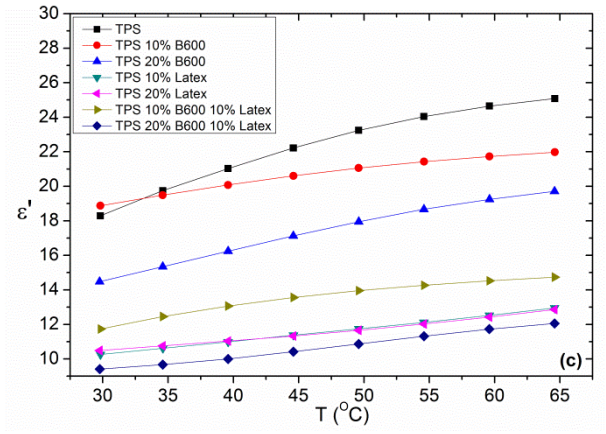

219

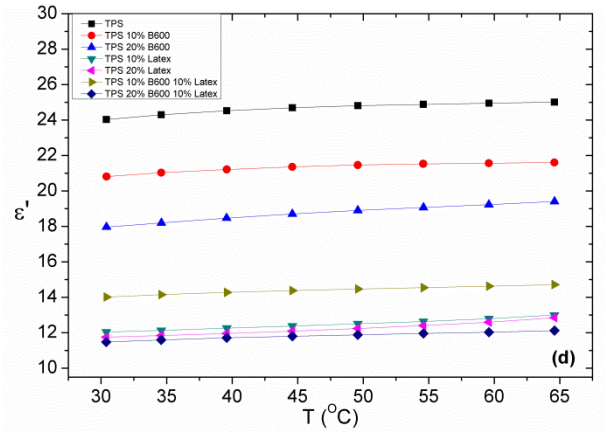

220

221 **Fig. 1:** The real part of dielectric permittivity as a function of temperature for all
222 specimens at: (a) 10^3 Hz, first thermal cycle, (b) 10^3 Hz, second thermal cycle, (c) 10^6
223 Hz, first thermal cycle and (d) 10^6 Hz, second thermal cycle.
224
225 Polarization and ε' attain high values at low frequencies since permanent and induced
226 dipoles acquire sufficient time to be aligned parallel to the field (Figs 1a and b).
227 Dipoles orientation is a thermally assisted process and thus permittivity increases, in
228 general, with temperature. In Fig. 1a and Fig. 1b it can be seen that the cellulose
229 reinforced composites exhibit the highest values of ε' throughout the whole
230 temperature spectrum at 10^3 Hz. As both cellulose and starch (amylose and
231 amylopectin) consist of glucose units (which have four hydroxyl groups and a
232 methylol group (-CH_2OH) linked to the main chain), they have very similar chemical
233 formulae but different three-dimensional structures. Since cellulose is a linear
234 macromolecule, it is easier to be aligned with the applied electric field than amylose
235 and amylopectin, resulting thus to higher values of polarization and ε' (Fig. 1a).
236 Cellulose and amylose are hydrophilic molecules due to the high concentrations of
237 hydroxyl groups and their 3D form. As cellulose is a linear macromolecule and
238 amylose is quasi-linear in a helical form, they exhibit differences in their hydrophilic
239 behavior. In the case of amylose, less hydroxyl groups are participating in the
240 intramolecular hydrogen bonds with water molecules, and as such, it is less
241 hydrophilic than cellulose. The enhanced hydrophilic character of cellulose results in
242 the attraction of water molecules, causing an obstruction to the motion of the polymer
243 chains. It should be considered that cellulose is a semi-crystalline polymer and its
244 crystallinity could exert restrictions to cellulosic chains mobility. Crystalline regions,
245 in semi-crystalline polymers, typically constrain amorphous parts of the polymer, due

246 to their rigidity leading to higher values of glass to rubber transition temperature.
247 Enhancement of T_g with the increase of cellulose (B600) has been confirmed via
248 DMTA tests in a previous work (Lendvai et al., 2016). However, the presence of
249 cellulose in the hybrid composites, in the same tests, didn't lead to an increase of T_g,
250 indicating that the presence of interfaces allows hydrophilicity to have a stronger
251 effect upon the resulting electrical polarization. Moreover, amorphous parts, because
252 of the absence of long range order, might favor the water penetration between chains
253 and thus the interactions, which result in the formation of H-bonds. So, the effect of
254 cellulose crystallinity in the relative systems is not considered as predominant.
255 Hence, although cellulose is aligned easier with the electric field than starch, higher
256 cellulose concentrations attract more water molecules leading to a hindrance of the
257 polar groups' orientation. Thus, the 10% B600 reinforced specimen attains higher
258 values of ε' compared to the 20% B600 sample. On the other hand, NR (latex) is a
259 hydrophobic non polar material exhibiting lower values of dielectric permittivity than
260 the TPS matrix (Psarras et al., 2007). In the NR latex modified composites two
261 competitive procedures are present. The significantly lower values of ε' for NR
262 compared to TPS lead to a decrement of the overall permittivity of the corresponding
263 composites. On the other hand, with increasing the latex concentration the
264 hydrophobic character of the composites becomes more prominent. Thus, the density
265 of H-bonds, and consequently the exerted obstructions to the orientation of the starch
266 macromolecules parallel to the electric field diminish. As a result the presence of 10%
267 latex in TPS matrix causes an initial reduction of dielectric permittivity, due to its low
268 values, which is countered back with the increase of latex content (20% latex),
269 because of the facilitation of system's polar groups to be oriented with the applied
270 field. Thus the reduction of H-bonds leads to a secondary increase of ε' (Fig. 1a).

In the case of the hybrid (i.e. microfibrillated cellulose + NR latex) composites low ε' values have been observed, and all the above mentioned influences are active. It is believed that due to higher concentrations of both modifiers more water is trapped between the TPS matrix and the cellulose reinforcement yielding enhanced interfacial interactions. When water molecules are near to amylose or cellulose macromolecules, H-bonds are formed causing an obstruction to the movement of polar groups with the applied electric field. Between the first and the second thermal cycle, Fig. 1a and 1b respectively, an increase in ε' has been observed only in temperatures up to 50^{o}C due to water evaporation. At higher temperatures, after water removal, no significant difference has been observed between the first and second cycles. In Fig. 1c and 1d, the highest values of ε' belong to starch macromolecules. In this frequency (10^6 Hz) a secondary and weaker polarization effect occurs due to the orientation of smaller polar segments, like free hydroxyl groups (not forming H-bonds). Although starch and cellulose possess equal number of hydroxyl groups, they differ in the number of the formed H-bonds between hydroxyl groups and water molecules, as mentioned previously. Amylose and amylopectin contain a greater amount of free hydroxyl groups than cellulose and as such, TPS exhibits higher values of ε' than the cellulose reinforced composites. Latex modified TPS and the hybrids exhibit lower ε' values as latex contains no hydroxyl groups at all and is a low permittivity material. At 10^6 Hz, the difference in ε' values between the first and second thermal cycle, is more intense at temperatures below 50^{o}C, as in the case of 10^3 Hz.

Fig. 2a presents the dependence of the imaginary part of electric modulus (M'') upon frequency at 30^{o}C for the first thermal cycle. The loss index of electric modulus forms a peak at medium to high frequencies, in all examined samples, which is attributed to

the glass to rubber transition of the polymer matrix, also noted as α-relaxation. A shoulder also appears at relatively lower frequencies, in the intermediate frequency range, which is attributed to a matrix-water-reinforcement interfacial polarization (MWR-IP). Water molecules lie in the interface between TPS and cellulose, where unbounded charges are also present. Thus, the resulting interfacial phenomena are related to dipole-dipole and dipole-charge interactions. Consequently, H-bonds are formed between the hydroxyl groups of glucose units of both starch and cellulose macromolecules. This phenomenon languishes as the temperature rises until most of the water is evaporated. The latter is clear in Fig. 2b which shows the imaginary part of electric modulus at 30^{o}C for the second thermal cycle, where no MWR-IP is observed and only the peak of α-relaxation is recorded. From Fig. 2a it is obvious that MWR-IP is characterized by a longer relaxation time, compared to α-relaxation, since it is recorded at lower frequencies.

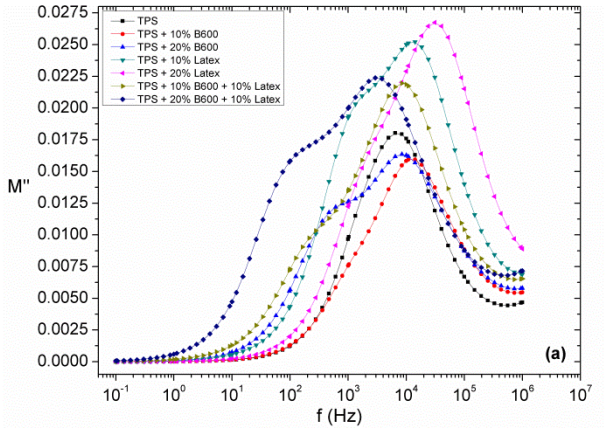

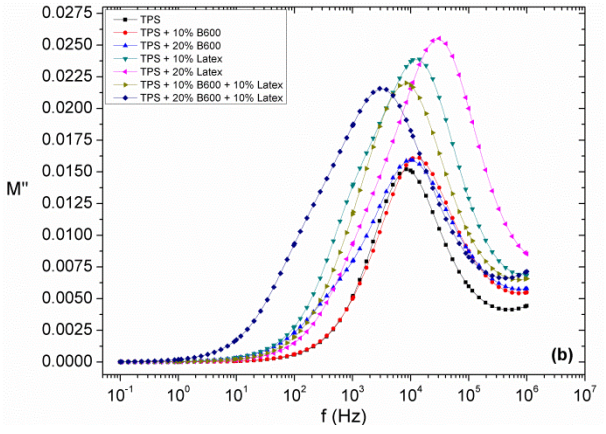

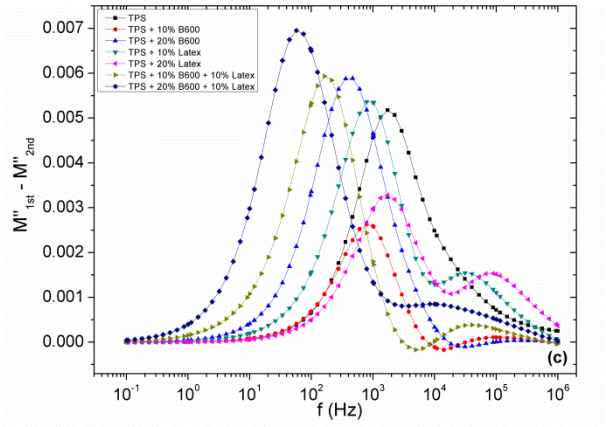

311

312 **Fig. 2:** The imaginary part of electric modulus for all specimens as a function of
313 frequency at 30ºC, for the: (a) first, (b) second thermal cycle, and (c) spectra
314 subtraction between the first the second thermal cycle.

315

316 Fig 2c depicts the subtraction of the loss modulus spectra prior and after water
317 removal (i.e. the "dry" spectra of Fig. 2b are subtracted from the corresponding
318 spectra of Fig. 2a). It is reasonable to consider that the remaining spectra of Fig. 2c
319 represent the contribution of water. The recorded processes appear to be weaker than
320 those present in the spectra of the first and the second cycle, and the main peak is
321 recorded very close to the frequency range where the MWR-IP shoulders are observed
322 in the loss curves of the first thermal cycle. Interestingly another relaxation process is
323 present, in the spectra of Fig. 2c, at the high frequency edge. This process appears to
324 be more intense in the case of the composites modified with the hydrophobic NR
325 latex, while is significantly weaker in the case of the hydrophilic cellulose reinforced
326 composites. The same process in hybrid composites exhibits an intermediate and
327 rather broad performance, since both hydrophilic and hydrophobic reinforcements co-
328 exist. The physical origin of this dielectric process could be ascribed to the polarity of
329 unbounded or free water molecules. Unlike hydrophilic inclusions, hydrophobic
330 fillers favor the presence of unbounded water molecules and thus the onset of the

corresponding dielectric process. The intermediate behavior of hybrid composites supports the previous interpretation since it can be considered as the superposition of two influences acting at opposite directions. This process although it should be present in the spectra of Fig. 2a, prior of water removal, it is hidden under the stronger effect of α-relaxation.

DSC thermographs (not shown here) recorded under two identical thermal cycles with the BDS tests indicate the evaporation of water upon heating in the first run, although no evidence for the initial location (interface or matrix) of water could be extracted.

3.2. Molecular dynamics

Fig. 3 shows the loss peak positions of the observed relaxation phenomena as a function of reciprocal temperature, prior and after water evaporation (i.e. first and second cycle, respectively). Fig. 3a presents the loss peak positions of both α-relaxation and MWR-IP. MWR-IP is easily observed only up to 45ºC, because of water evaporation. Matrix-water-cellulose reinforcement interfacial polarization and Maxwell-Wagner-Sillars effect exhibit a set of common characteristics including longer relaxation time than the α-mode, Arrhenius temperature dependence and relation to interfacial phenomena. The loss peak positions after water evaporation (second thermal cycle) are depicted in Fig. 3b, where only α-relaxation is observed.

The temperature dependence of the MWR-IP peaks maxima can be described by the Arrhenius relation (cf. Equation 3):

$$f_{max} = f_0 e^{-\frac{E_A}{k_B T}} \quad (3)$$

where f_0 is a pre-exponential factor, E_A is the activation energy, k_B the Boltzmann constant and T the absolute temperature. On the other hand, the temperature dependence of α-relaxation obeys the Vogel-Fulcher-Tammann (VFT) relation – cf. Equation 4:

$$f_{max} = f_0 e^{-\frac{AT_0}{(T-T_0)}} \quad (4)$$

where f_0 is a pre-exponential factor, A a constant being the measure of activation energy, T_0 the Vogel temperature or ideal glass transition temperature and T the absolute temperature. The fitting parameters of Arrhenius and VFT equations to the experimental data are given in Table 2. It should be noted, that recorded data did not lead to reliable fittings for the MWR-IP process in all specimens. These cases are omitted from both Fig. 3 and Table 2.

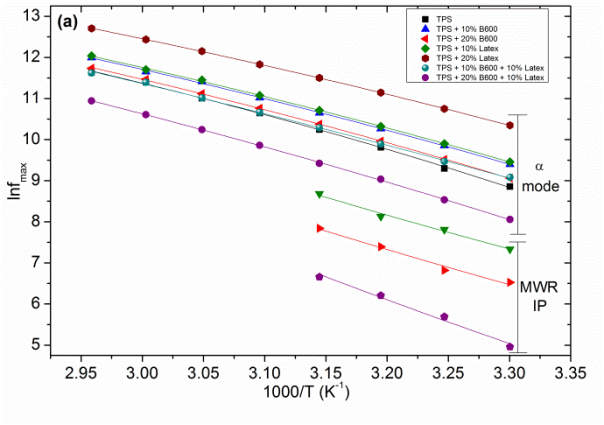

375

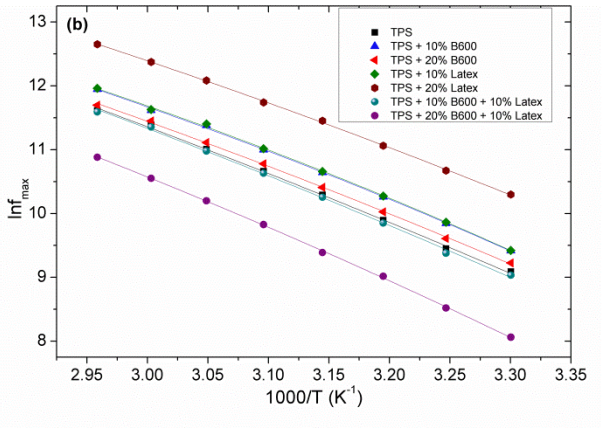

376

377 **Fig. 3:** Loss peak position of the recorded relaxations, as a function of reciprocal
378 temperature for the: (a) first and (b) second thermal cycle.

379

380 **Table 2:** Activation energy for matrix-water-reinforcement-interfacial polarization
381 and Vogel parameters for α-relaxation for both thermal cycles.

382

383

384

385

386

387

388

Specimen	MWR-IP	α-mode			
		1st cycle		2nd cycle	
	E_A (eV)	A	T_0 (K)	A	T_0 (K)
TPS	-	0.240	234.62	0.437	207.01
TPS+10% B600	-	0.287	223.00	0.285	222.39
TPS+20% B600	0.780	0.276	227.09	0.371	212.27
TPS+10% Latex	0.750	0.279	223.64	0.264	225.43
TPS+20% Latex	-	0.278	217.55	0.352	207.99
TPS+10% B600+ 10% Latex	-	0.446	206.14	0.422	209.41
TPS+20% B600+ 10% Latex	0.949	0.351	224.14	0.360	222.48

VFT parameters are highly affected when the evaporated water molecules were acting as plasticizing agents. Thus, the stronger effect is observed in the case of the TPS sample. T_0 values shift to lower values, as expected, with the evaporation of plasticizing water molecules, since the TPS polymer chains achieve increased mobility, because of the reduction of restricting the H-bonds, and the relative relaxation process is facilitated. The same trend has been observed in the actual T_g value of the systems, as determined via DMTA studies (Lendvai et al., 2016). The variations of parameter A are in accordance with those of T_0, since parameter A reflects the required amount of activation energy for the glass to rubber transition process.

Values of activation energy E_A for the MWR-IP process are higher in the case of TPS/cellulose composites than in the case of TPS/latex ones, since cellulose is

hydrophilic and latex is hydrophobic and thus water molecules are stronger bonded at the interface in the first case. Notably, the system with the highest heterogeneity (TPS+20% B600+ 10% Latex) exhibits the highest value of E_A. Trapped water molecules between the interfaces of the constituents restricted by the interactions with cellulose and amylose, and their ability to be polarized with the field diminishes.

3.3. Energy density and dielectric reinforcing function

Fig. 4 presents the energy density and the normalized energy density as a function of frequency for all specimens at constant electric field E = 1 kV/m, at 30ºC. Energy density is defined via Equation (5), as follows:

$$U = \frac{1}{2}\varepsilon_0 \varepsilon' E^2 \qquad (5)$$

where ε_0 is the permittivity of free space and E the intensity of the applied electric field. From Equation (5) it is apparent that energy density is highly affected by the electric field, being also limited by its maximum value at the dielectric breakdown. However, the only material property influencing energy density is the real part of dielectric permittivity.

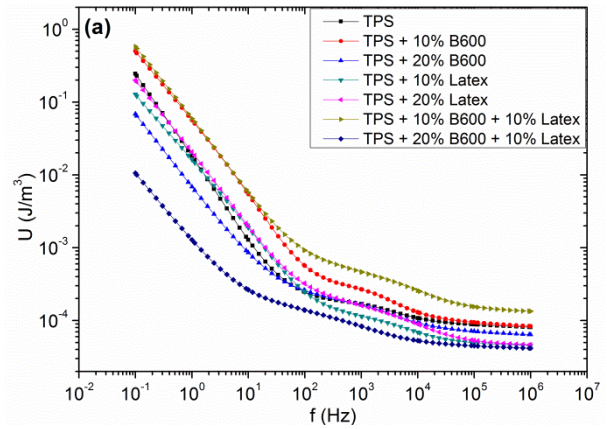

418

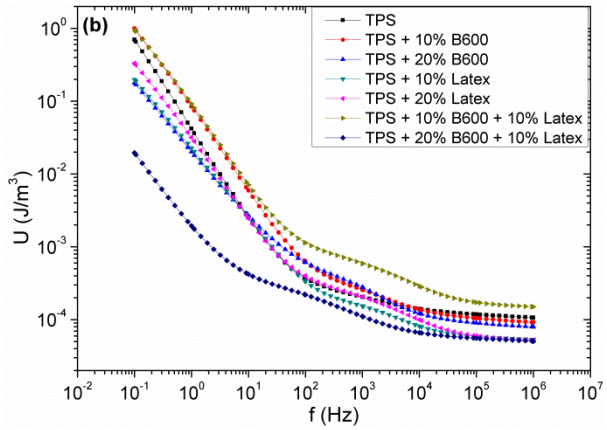

419

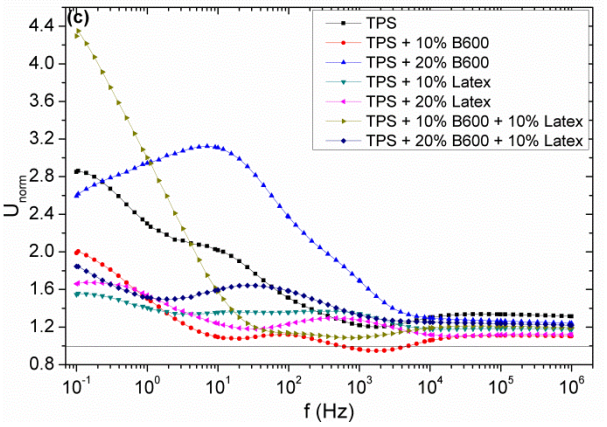

420

421 **Fig. 4:** Energy density as a function of frequency for all specimens at constant electric
422 field E = 1 kV/m at 30ºC, (a) prior and (b) after water evaporation. (c) Normalized
423 energy density as a function of frequency for all specimens.

424

425 Normalized energy density is defined according to Equation (6):

426

427 $$U_{norm} = \frac{U_{2nd}}{U_{1st}} \qquad (6)$$

where U_{2nd} and U_{1st} are the values of energy density for the second and first thermal cycle, respectively.

Fig. 4a presents the energy density for the first thermal cycle while Fig. 4b for the second one. As expected, energy density at constant field follows the variation of ε' and at low frequencies it attains high values. In medium frequency range, ε' values are less dependent on frequency until they reach almost constant values at the high frequency edge. Step-like transitions from high to low values of energy density at intermediate frequencies imply the role of α-relaxation process. From both Fig. 4a and 4b, it is evident that the specimens with the lowest energy density values are those with the most intense presence of MWR-IP (cf. Fig 3). This is attributed to the intra-molecular hydrogen bonds formed between water molecules and hydroxyl group of the TPS chain and as a result reduces polarization and thus ε'. On the other hand, the specimens of TPS + 10% B600 and TPS + 10% B600 + 10% Latex which had relatively low water concentration (Fig. 2a), exhibit the highest values, rising up to 1 J/m^3 at 10^{-1} Hz. Furthermore the TPS energy density seems not to be affected by the presence of latex modification. Fig. 4c shows that all specimens after water evaporation exhibit 1.5 to 4.4 times higher values of energy density at low frequencies at 30^{o}C. Evaporation of water minimizes the hydrogen bonds between water molecules and hydroxyl side groups of the main polymer chains, and thus reduces the exerted mobility restrictions. Hence, system's polarization becomes easier since polar groups are facilitated in their alignment to the field and therefore the real part of dielectric permittivity gets higher values.

Dielectric Reinforcing Function (DRF) is defined according to Equation (7):

$$G(f,T) = \frac{\varepsilon'_{comp}(f,T)}{\varepsilon'_{mat}(f,T)} \quad (7)$$

where $\varepsilon'_{comp}(f,T)$ and $\varepsilon'_{mat}(f,T)$ is the real part of dielectric permittivity of the composite and the matrix respectively, while f is the frequency of the field and T the temperature (Ioannou, Patsidis, & Psarras, 2011). It should be noted that TPS is considered as the matrix. DRF is a dimensionless function being a measure of the normalized polarization, upon the geometrical characteristics of the samples, and the dielectric strengthening ability of the modifier. Additionally, DRF offers a strong indication relative to the energy storing efficiency of the composites (Ioannou et al., 2011; Patsidis, & Psarras, 2013).

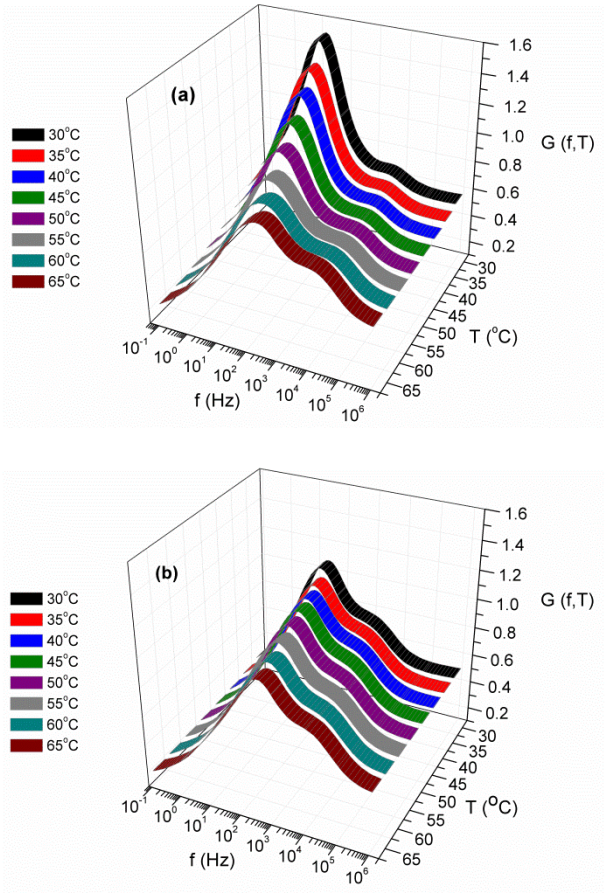

Fig. 5: DRF as a function of frequency and temperature for TPS + 10% Latex for the: (a) first and (b) second thermal cycle.

Fig. 5 presents the variation of DRF with temperature and frequency for TPS + 10% Latex. Fig. 5a shows the first thermal cycle where two processes are recorded. There is one peak at low to medium frequencies, which is indicative of the existence of water and also another process at higher frequencies which indicates α-relaxation. As the temperature rises, DRF values for the water-related peak fall and stabilize at 60 and 65ºC, when all water is assumed as evaporated. The remaining peak could be attributed to interfacial polarization between the composite's constituents and possibly to a trapped limited quantity of water. In the second thermal cycle, as Fig. 5b shows, the DRF values for the water-related peak are stable in the whole temperature range, since water has been evaporated, and thus only the interfacial phenomena are at work. The DRF values for α-relaxation in Fig. 5a differ only at lower temperatures, compared to Fig. 5b, as water molecules slightly affect the α-mode. Limited quantity of water molecules absorbed by the TPS matrix evaporate by heating leading to a variation of the Vogel temperature (Table 2).

3.4. Environmental exposure

Fig. 6 presents the imaginary part of electric modulus as a function of frequency at 30ºC for the TPS + 20% B600 sample. After the second thermal cycle, the specimen was exposed to ambient temperature and humidity conditions for 120 hours prior to a third testing cycle. The third thermal cycle shows that part of the adsorbed water was retrieved during the environmental exposure. The loss peak at 10^2 Hz indicates the existence of that water. This peak is evident in the spectra of the first cycle and the third thermal cycles. In the first one the high water concentration results from the specimen's manufacturing process, while in the third cycle retrieved water originates

from the environmental exposure. Obviously, this peak is absent in the spectrum of the second thermal cycle, since water has been evaporated.

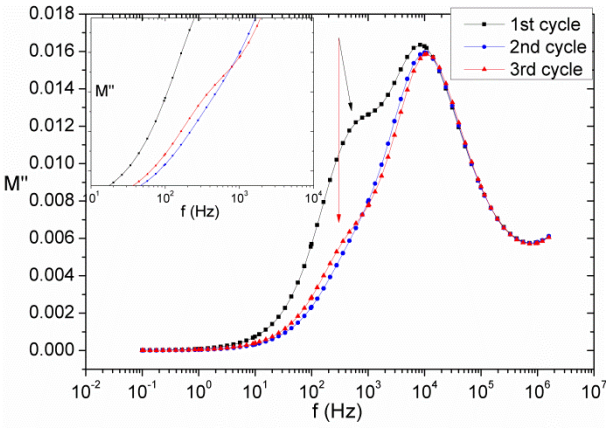

Fig. 6: Imaginary part of electric modulus as a function of frequency at 30ºC for TPS + 20% B600 for the first, the second and the third thermal cycle.

4. Conclusion

The effect of water on the dielectric properties and electrical conductivity of thermoplastic starch (TPS) modified with microfibrillated cellulose and natural rubber latex microparticles was investigated in the present study. Dielectric permittivity increases with frequency decrement, temperature rise and cellulose content. Electric modulus loss spectra during the first thermal cycle indicate the presence of two relaxation processes, which are attributed to MWR-IP and glass to rubber transition (α-relaxation). MWR-IP relaxation process is assigned to the existence of water molecules between the polymer chains and constituents. This relaxation process diminishes as temperature rise until all water is evaporated. Relaxation dynamics of α-mode process appear to be weakly affected at low temperatures from water content. Energy density increases as frequency falls and also during water evaporation. The influence of temperature is very important on water content. Hence, the dielectric

behavior of the specimens varies according to the filler's nature (hydrophilic or hydrophobic) and concentration, as well as the sample's treatment. Finally, it was observed that evaporated water can be partially retrieved inside the composites, under proper environmental conditions, indicating that the effect of absorption/evaporation is reversed. Hence, TPS biocomposites modified with microfibrillated cellulose and latex microparticles could be considered as functional materials exhibiting sensing capabilities.

Acknowledgement

The work reported here was supported by the Hungarian Research Fund (OTKA) through the project K 109409.

References

Arous, M., Ben Amor I., Boufi, S., & Kallel, A. (2007). Experimental study on dielectric relaxation in alfa fiber reinforced epoxy composites. *Journal of Applied Polymer Science, 106,* 3631-3640.

Bugnicourt, E., Cinelli, P., Lazzeri, A., & Alvarez, V. (2014). Polyhydroxyalkanoate (PHA): Review of synthesis, characteristics, processing and potential applications in packaging. *Express Polymer Letters, 8,* 791-808.

Chen, B., & Evans, J. R. G. (2005). Thermoplastic starch-clay nanocomposites and their characteristics. *Carbohydrate Polymers, 6,* 455-463.

Chung, Y.-L., Ansari, S., Estevez, L., Hayrapetyan, S., Giannelis, E. P., & Lai, H.-M. (2010). Preparation and properties of biodegradable starch-clay nanocomposites. *Carbohydrate Polymers, 79,* 391-396.

537 Dean, K., Yu, L., & Wu, D. Y. (2007). Preparation and characterization of melt-
538 extruded thermoplastic starch/clay nanocomposites. *Composites Science and*
539 *Technology, 67,* 413-421.
540 Gatos, K. G., Martínez Alcázar, J. G., Psarras, G. C., Thomann, R., & Karger-Kocsis,
541 J. (2007). Polyurethane latex/water dispersible boehmite alumina nanocomposites:
542 Thermal, mechanical and dielectrical properties. *Composites Science and Technology,*
543 *67,* 157-167.
544 Herculano, R. D., Silva, C. P., Ereno, C., Guimaraes, S. A. C., Kinoshita, A., &
545 Graeff, C. F. O. (2009). Natural rubber latex used as drug delivery system in guided
546 bone regeneration (GBR). *Materials Research, 12,* 253-256.
547 Ioannou, G., Patsidis, A., & Psarras, G. C. (2011). Dielectric and functional properties
548 of polymer matrix/ZnO/$BaTiO_3$ hybrid composites. *Composites: Part A: Applied*
549 *Science and Manufacturing, 42,* 104-110.
550 Iqbal, H. M. N., Kyazze, G., Locke, I. C., Tron, T., & Keshavarz, T. (2015).
551 Development of novel antibacterial active, HaCaT biocompatible and biodegradable
552 CA-g-P(3HB)-EC biocomposites with caffeic acid as a functional entity. *Express*
553 *Polymer Letters, 9,* 764-772.
554 Kamel S. (2007). Nanotechnology and its applications in lignocellulosic composites, a
555 mini review. *Express Polymer Letters, 1,* 546-575.
556 Karger-Kocsis, J., Kmetty, Á., Lendvai, L., Drakopoulos, S. X., & Bárány, T. (2015).
557 Water-assisted production of thermoplastic nanocomposites: A review. *Materials, 8,*
558 72-95.
559 Kmetty, Á., Karger-Kocsis, J., & Czigány, T. (2015). Production and properties of
560 micro-cellulose reinforced thermoplastic starch. *IOP Conference Series: Materials*
561 *Science and Engineering, 74,* 012008.

562 Kremer F., & Schönhals A. (2009). Broadband dielectric measurement techniques
563 (10^{-6} Hz to 10^{12} Hz). In F. Kremer, & A. Schönhals (Eds.), *Broadband dielectric*
564 *spectroscopy* (pp. 35-64) Springer, Berlin.
565 Ladhar, A., Arous, M., Kaddami, H., Raihane, M., Kallel, A., Graça, M. P. F., et al.
566 (2014). Molecular dynamics of nanocomposites natural rubber/cellulose nanowhiskers
567 investigated by impedance spectroscopy. *Journal of Molecular Liquids, 196,* 187-191.
568 Lendvai, L., Karger-Kocsis, J., Kmetty, Á., & Drakopoulos, S. X. (2016). Production
569 and characterization of microfibrillated cellulose-reinforced thermoplastic starch
570 composites. *Journal of Applied Polymer Science, 133,* 42397.
571 Liu, H., Xie, F., Yu, L., Chen, L., & Li, L. (2009). Thermal processing of starch-based
572 polymers. *Progress in Polymer Science, 34,* 1348-1368.
573 Majdzadeh-Ardakani, K., Navarchian, A. H., & Sadeghi, F. (2010). Optimization of
574 mechanical properties of thermoplastic starch/clay nanocomposites. *Carbohydrate*
575 *Polymers, 79,* 547-554.
576 Mano, J. F., Koniarova, D., & Reis, R. L. (2003). Thermal properties of thermoplastic
577 starch/ synthetic polymer blends with potential biomedical applicability. *Journal of*
578 *Materials Science: Materials in Medicine, 14,* 127-135.
579 Nafchi, A. M., Moradpour, M., Saeidi, M., & Alias, A. K. (2013). Thermoplastic
580 starches: Properties, challenges, and prospects. *Starch, 65,* 61-72.
581 Nasseri, R., & Mohammadi, N. (2014). Starch-based nanocomposites: A comparative
582 performance study of cellulose whiskers and starch nanoparticles. *Carbohydrate*
583 *Polymers, 106,* 432-439.
584 Ortiz-Serna, P., Carsí, M., Redondo-Foj, B., & Sanchis, M. J. (2014). Electrical
585 conductivity of natural rubber-cellulose II nanocomposites. *Journal of Non-*
586 *Crystalline Solids, 405,* 180-187.

587 Patsidis, A. C., & Psarras, G. C. (2013). Structural transition. dielectric properties and
588 functionality in epoxy resin-barium titanate nanocomposites. *Smart Materials and*
589 *Structures, 22,* 115006.
590 Psarras, G. C., Gatos, K. G., Karahaliou, P. K., Georga, S. N., Krontiras, C. A., &
591 Karger-Kocsis J. (2007). Relaxation phenomena in rubber/layered silicate
592 nanocomposites. *Express Polymer Letters, 1,* 837-845.
593 Psarras, G. C., Gatos, K. G., & Karger-Kocsis, J. (2007). Dielectric properties of
594 layerd silicate-reinforced natural and polyurethane rubber nanocomposites. *Journal of*
595 *Applied Polymer Science, 106,* 1405-1411.
596 Rolere, S., Bottier, C., Vaysse, L., Sainte-Beuve, J., & Bonfils, F. (2016).
597 Characterisation of macrogel composition from industrial natural rubber samples:
598 Influence of proteins on the macrogel crosslink density. *Express Polymer Letters, 10,*
599 408-419.
600 Rose K., & Steinbüchel A. (2005). Biodegradation of natural rubber and related
601 compounds: Recent insights into a hardly understood catabolic capability of
602 microorganisms. *Applied Environmental Microbiology, 71,* 2803-2812.
603 Ruellan, A., Guinault, A., Sollogoub, C., Chollet, G., Ait-Mada, A., Ducruet, V., et al.
604 (2015). Industrial vegetable oil by-products increase the ductility of polylactide.
605 *Express Polymer Letters, 9,* 1087-1103.
606 Schlemmer, D., Angélica, R. S., & Sales, M. J. A. (2010). Morphological and
607 thermomechanical characterization of thermoplastic starch/montmorillonite
608 nanocomposites. *Composite Structures, 92,* 2066-2070.
609 Siengchin, S., Karger-Kocsis, J., Psarras, G. C., & Thomann, R. (2008).
610 Polyoxymethylene/polyurethane/alumina ternary composites: Structure, mechanical,

611 thermal and dielectric properties. *Journal of Applied Polymer Science, 110,* 1613-
612 1623.
613 Siengchin, S., Karger-Kocsis, J., & Thomann, R. (2008). Nanofilled and/or toughened
614 POM composites produced by water-mediated melt compounding: Structure and
615 mechanical properties. *Express Polymer Letters, 2,* 746-756.
616 Tábi T., & Kovács J. G. (2007). Examination of injection moulded thermoplastic
617 maize starch. *Express Polymer Letters, 1,* 804-809.
618 Tanrattanakul, V., & Bunkaew, P. (2014). Effect of different plasticizers on the
619 properties of bio-based thermoplastic elastomer containing poly(lactic acid) and
620 natural rubber. *Express Polymer Letters, 8,* 387-396.
621 Tsangaris, G. M., Psarras, G. C., & Kouloumbi, N. (1998). Electric modulus and
622 interfacial polarization in composite polymeric systems. *Journal of Materials*
623 *Science, 33,* 2027-2037.
624 Xie, F., Pollet, E., Halley, P. J., & Avérous, L. (2013). Starch-based nano-
625 biocomposites. *Progress in Polymer Science, 38,* 1590-1628.